

2D Gapless Topological Superfluids Generated by Pairing Phases

Jiapei Zhuang,¹ Ching-Yu Huang,² Po-Yao Chang,¹ and Daw-Wei Wang^{1,3,4,5}

¹*Department of Physics, National Tsing Hua University, Hsinchu 30013, Taiwan*

²*Department of Applied Physics, Tunghai University, Taichung 40704, Taiwan*

³*Frontier Center for Theory and Computation, National Tsing Hua University, Hsinchu 30013, Taiwan*

⁴*Physics Division, National Center for Theoretical Sciences, Taipei 10617, Taiwan*

⁵*Center for Quantum Technology, National Tsing Hua University, Hsinchu 30013, Taiwan*

(Dated: August 2, 2022)

We systematically investigate the ground state phase diagram and the finite temperature phase transitions for a Rydberg-dressed Fermi gas loaded in a bilayer optical lattice. When an effective finite-ranged attraction is induced, our self-consistent mean-field calculation shows that the gapped topological (p -wave) superfluids in each layer are coupled together by the s -wave pairing in an intermediate inter-layer distance with a spontaneously modulated phases between these two order parameters. The obtained ground state is a gapless topological superfluid with quantized topological charges characterizing the gapless points, leading to a zero energy flat band at the edges. Finally, we calculate the finite temperature phase diagrams of this two-dimensional gapless superfluid and observe two distinct critical temperatures, demonstrating the fruitful many-body effects on a paired topological superfluids.

I. INTRODUCTION

The existence of Majorana particles has been a long-standing and important subject in theoretical high-energy physics [1], because they are defined by their own antiparticles and hence have many special properties compared to other elementary particles. In condensed matter physics, however, Majorana particles are referred to the quasiparticles emerging on the edge of a topological superfluid, called Majorana zero modes (MZM). MZMs obey non-Abelian statistics and hence are expected to be the major player for a fault-tolerant quantum computer [2–4]. Recent rapid development on the proposal and observation of Majorana zero modes has drawn a lot of attentions in the field of condensed matter physics [5].

To realize topological superconductors supporting Majorana zero modes, many theoretical models [6–8] and experimental systems were proposed in recent years, including nanowires in contact with the superconductors [9], quantum anomalous Hall insulator/superconductor hybrid devices [10], quantum spin liquids [11], iron-based superconductors [12], and so on. However, the experimental evidences are still unclear and some of them face repeatable crises [13, 14].

The development of experiment techniques in ultracold atoms suggest other possible scenario to realize Majorana zero modes in the systems of topological superfluids [15–19]. Moreover, the quantum gases made by Rydberg-dressed atoms further open up new possibilities to study various topological phases, because the effective dipole moments, interaction strength and even the interaction range are all tunable in a wide parameter regime. In fact, many interesting many-body ground states have been predicted in different magneto-optical traps, including a two-dimensional (2D) layer, bi-layer and multi-layer systems [20–27].

In this paper, we consider a bi-layer system with a Rydberg-dressed Fermi gas. We focus on the parameter region where the effective finite-ranged interaction are attractive in all directions. Minimizing the total energy with respect to both the amplitudes and phases of these order parameters within the self-consistent mean-field approximation, we find that the

systems can host superfluid state with s -wave pairing, p -wave pairing, and a mixture of them. For the latter case, the pairing phases of these two p -wave in the two layers has a phase difference π , and gapless points emerge in the bulk energy spectrum. We characterize each point by calculating the quantized winding number around them and show how the zero-energy flat bands emerge at the edges spectrum. We emphasize that such a gapless topological superfluid results from a specific pairing phase locking between the co-existing s -wave and p -wave pairing order parameters, and therefore were not considered in the literature before. We further show how these two order parameters co-exist and influence each other in the finite temperature regime.

The article is organized as follows. In Sec. II, we introduce the Hamiltonian for a Fermi gas loaded into a 2D bi-layered system with the Rydberg-dressing interaction. In Sec. III, we derive the mean-field Hamiltonian with both the amplitudes and phases of the pairing order parameters. In Sec. IV, we calculate the ground state energy through variational methods and show the obtained quantum phase diagram. In Sec. V, we demonstrate that a non-trivial phase between the s -wave and the p -wave is a topological superfluid with a finite winding number at the gapless points, leading to localized zero energy models at the edge. In Sec. VI, we calculate the critical temperature of the gapless topological superfluid with two order parameters, and then summarize our results in Sec. VII.

II. PHYSICAL SYSTEM AND HAMILTONIAN

A. Rydberg-dressed Interaction

We consider a 2D bi-layer system with a square optical lattice within the $x - y$ plane (see Fig. 1(a)), where a single-species Fermi gas is loaded with finite tunneling amplitudes between lattice sites in the same or opposite layers. As a result, the system could also be effectively understood as a 2D pseudo-spin 1/2 system with an effective in-plane magnetic field via the inter-layer tunneling. In order to generate

an effective interaction between these single-species fermions, an off-resonant two-photon transition is introduced to weakly couple the electronic ground state to a Rydberg excited state via an intermediate state. In the far detuning and weak coupling limit, it is known that the effective Rydberg-dressed interaction between these dressed-state atoms could be approximated by a finite ranged soft-core interaction (see Fig. 1(b)): $V_{RD}(\mathbf{r}) = \frac{U_0}{1+(r/R_c)^6}$ within the standard perturbation and adiabatic approximation [28–33]. Here the effective interaction strength, U_0 , and the interaction range, R_c , could be calculated explicitly from the Rabi coupling and detuning from the atomic excitations [28]. Many proposals discussed how to manipulate such a Rydberg-dressed interaction via various external fields [34, 35].

We focus on the parameter regime to generate an effective attraction ($U_0 < 0$) and a finite-ranged Rydberg blockade radius ($R_c \sim a, d$, with a and d being the intra-layer and inter-layer lattice spacing respectively). As a result, these single-species fermions could be effectively interacting with each other with the following Hamiltonian in real space

$$\begin{aligned} \hat{H} = & -t \sum_{\mathbf{r}, \sigma} [\hat{c}_{\mathbf{r}, \sigma}^\dagger \hat{c}_{\mathbf{r}+\hat{x}, \sigma} + \hat{c}_{\mathbf{r}, \sigma}^\dagger \hat{c}_{\mathbf{r}+\hat{y}, \sigma} + h.c.] \\ & -t_z \sum_{\mathbf{r}, \sigma} \hat{c}_{\mathbf{r}, \sigma}^\dagger \hat{c}_{\mathbf{r}, -\sigma} - \mu \sum_{\mathbf{r}, \sigma} \hat{c}_{\mathbf{r}, \sigma}^\dagger \hat{c}_{\mathbf{r}, \sigma} \\ & -\frac{1}{2} \sum_{\mathbf{r}, \mathbf{r}', \sigma} V_{\parallel}(\mathbf{r} - \mathbf{r}') \hat{c}_{\mathbf{r}, \sigma}^\dagger \hat{c}_{\mathbf{r}', \sigma}^\dagger \hat{c}_{\mathbf{r}', \sigma} \hat{c}_{\mathbf{r}, \sigma} \\ & -\frac{1}{2} \sum_{\mathbf{r}, \mathbf{r}', \sigma} V_{\perp}(\mathbf{r} - \mathbf{r}') \hat{c}_{\mathbf{r}, \sigma}^\dagger \hat{c}_{\mathbf{r}', -\sigma}^\dagger \hat{c}_{\mathbf{r}', -\sigma} \hat{c}_{\mathbf{r}, \sigma} \end{aligned} \quad (1)$$

where $\hat{c}_{\mathbf{r}, \sigma}^\dagger$ ($\hat{c}_{\mathbf{r}, \sigma}$) is the creation(annihilation) operator of fermions with the layer index $\sigma = (\uparrow, \downarrow)$, μ is the chemical potential, and $\mathbf{r} = (i_x, i_y)$ is the in-plane coordinate. The intra-layer and inter-layer tunnelling amplitude are t and t_z respectively. Both tunneling amplitudes can be tuned independently by the lattice strength and lattice spacing. Here $V_{\perp}(\mathbf{r} - \mathbf{r}')$ and $V_{\parallel}(\mathbf{r} - \mathbf{r}')$ are the interlayer and intra-layer interaction provided by the Rydberg-dressed interaction, $V_{RD}(\mathbf{r})$, and defined positively for the convenience of latter discussion.

B. BCS mean-field Approximation

To investigate the topological features, we further apply Fourier transform of the field operator, $\hat{c}_{\mathbf{r}, \sigma} = \frac{1}{\Omega} \sum_{\mathbf{k}} \hat{c}_{\mathbf{k}, \sigma} e^{i\mathbf{k} \cdot \mathbf{r}}$, to transform the Hamiltonian into the momentum space and apply the BCS mean-field approximation between pairs of fermions. Here Ω is the system area. It is well-known that the resulting mean-field Hamiltonian (\hat{H}_{MF}) can be written to be a 4×4 matrix form within the Nambu spinor representation, $\hat{\Psi}_{\mathbf{k}} \equiv [\hat{c}_{\mathbf{k}\uparrow}, \hat{c}_{\mathbf{k}\downarrow}, \hat{c}_{-\mathbf{k}\uparrow}^\dagger, \hat{c}_{-\mathbf{k}\downarrow}^\dagger]^T$, and the final results can be divided in two parts: $\hat{H}_{MF} = \hat{H}_{BCS} + E_c$,

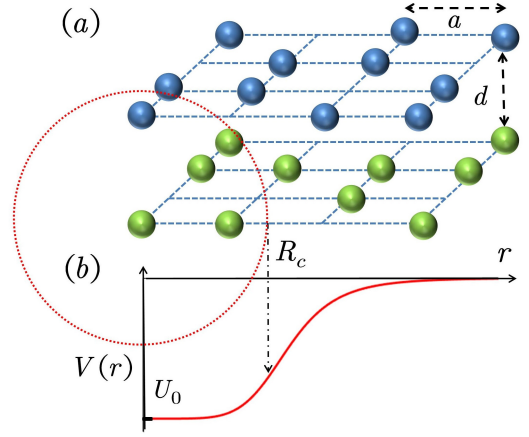


FIG. 1: (a) The bilayer structure with a single species Fermi gas discussed in this work. A square optical lattice potential is applied inside the layer ($x - y$) plane with a and d being the intra-layer and inter-layer lattice spacing respectively. The blue/green objects indicate fermionic Rydberg atoms loaded in the upper/lower layer. (b) The obtained effective Rydberg-dressed interaction, $V_{RD}(r)$ between these fermionic atoms with a soft-core strength, U_0 and a finite blockade radius R_c . See the text.

where

$$\hat{H}_{BCS} = \frac{1}{2} \sum_{\mathbf{k}} \hat{\Psi}_{\mathbf{k}}^\dagger \begin{bmatrix} \varepsilon_{\mathbf{k}} & -t_z & 2\Delta_{p\uparrow}^* & \Delta_s^* \\ -t_z & \varepsilon_{\mathbf{k}} & -\Delta_s^* & 2\Delta_{p\downarrow}^* \\ 2\Delta_{p\uparrow} & -\Delta_s & -\varepsilon_{\mathbf{k}} & t_z \\ \Delta_s & 2\Delta_{p\downarrow} & t_z & -\varepsilon_{\mathbf{k}} \end{bmatrix} \hat{\Psi}_{\mathbf{k}} \quad (2)$$

and the constant energy term is given by

$$\begin{aligned} E_c = & \frac{1}{\Omega} \sum_{\mathbf{k}, \mathbf{k}'} V_{\mathbf{k}, \mathbf{k}'}^\perp \langle \hat{c}_{\mathbf{k}', \uparrow}^\dagger \hat{c}_{-\mathbf{k}', \downarrow}^\dagger \rangle \langle \hat{c}_{-\mathbf{k}, \downarrow} \hat{c}_{\mathbf{k}, \uparrow} \rangle \\ & + \frac{1}{\Omega} \sum_{\mathbf{k}, \mathbf{k}'} V_{\mathbf{k}, \mathbf{k}'}^\parallel \langle \hat{c}_{\mathbf{k}', \uparrow}^\dagger \hat{c}_{-\mathbf{k}', \uparrow}^\dagger \rangle \langle \hat{c}_{-\mathbf{k}, \uparrow} \hat{c}_{\mathbf{k}, \uparrow} \rangle \\ & + \frac{1}{\Omega} \sum_{\mathbf{k}, \mathbf{k}'} V_{\mathbf{k}, \mathbf{k}'}^\parallel \langle \hat{c}_{\mathbf{k}', \downarrow}^\dagger \hat{c}_{-\mathbf{k}', \downarrow}^\dagger \rangle \langle \hat{c}_{-\mathbf{k}, \downarrow} \hat{c}_{\mathbf{k}, \downarrow} \rangle \\ & + 2 \sum_{\mathbf{k}} \varepsilon_{\mathbf{k}} \end{aligned} \quad (3)$$

with $\langle \dots \rangle$ being an expectation value and $\varepsilon_{\mathbf{k}} = -2t(\cos k_x + \cos k_y) - \mu$ being the bare kinetic energy. For simplicity, we use the layer index as the pseudo-spin index and define the inter-layer pairing order parameters to be the "s-wave" pairing (Δ_s) and the intra-layer pairing order to be the "p-wave" pairing (Δ_p). These order parameters could be calculated through the inter- and intra-layer interaction strength as following:

$$\Delta_s(\mathbf{k}) = \frac{1}{\Omega} \sum_{\mathbf{k}'} V_{\mathbf{k}, \mathbf{k}'}^\perp \langle \hat{c}_{-\mathbf{k}', \downarrow} \hat{c}_{\mathbf{k}', \uparrow} \rangle \quad (4)$$

$$\Delta_{p, \sigma}(\mathbf{k}) = \frac{1}{\Omega} \sum_{\mathbf{k}'} V_{\mathbf{k}, \mathbf{k}'}^\parallel \langle \hat{c}_{-\mathbf{k}', \sigma} \hat{c}_{\mathbf{k}', \sigma} \rangle \quad (5)$$

for $\sigma = \pm = \uparrow / \downarrow$. Here $V_{\mathbf{k},\mathbf{k}'}^{\parallel,\perp}$ is the Fourier transform of the intra-layer and the inter-layer interaction matrix elements $V_{\parallel,\perp}(\mathbf{r} - \mathbf{r}')$ respectively.

III. MEAN-FIELD GROUND STATE ENERGY

A. Ground State Energy

In order to calculate the ground state energy within the mean-field approximation, we first diagonalize the BCS mean-field Hamiltonian (Eq. (2)), and obtain the low energy excitations for the Bogoliubov quasi-particles:

$$\hat{H}_{BCS} = \frac{1}{2} \sum_{\mathbf{k}} \hat{\Gamma}_{\mathbf{k}} \begin{bmatrix} E_{1,\mathbf{k}} & 0 & 0 & 0 \\ 0 & E_{2,\mathbf{k}} & 0 & 0 \\ 0 & 0 & E_{3,\mathbf{k}} & 0 \\ 0 & 0 & 0 & E_{4,\mathbf{k}} \end{bmatrix} \hat{\Gamma}_{\mathbf{k}} \quad (6)$$

Note that, the inter-layer pairing could be in principle either s -wave (singlet) or p -wave (triplet). But the singlet pairing must be energetically more favorable, because its symmetric orbital wavefunction always lowered the attractive inter-layer interaction energy, similar to the systems of polar molecules with an electric field perpendicular to the layer plane [21, 22, 36]. On the other hand, the intra-layer pairing in the $x - y$ plane must be triplet since the orbital wavefunction in the momentum space must be anti-symmetric as shown in Eq. (5).

where $\hat{\Gamma}_{\mathbf{k}} \equiv [\hat{\gamma}_{1,\mathbf{k}}, \hat{\gamma}_{2,\mathbf{k}}, \hat{\gamma}_{3,-\mathbf{k}}, \hat{\gamma}_{4,-\mathbf{k}}]^T$ is the Nambu spinor in Bogoliubov eigemode basis with $E_{j,\mathbf{k}}$ ($j = 1, \dots, 4$) being their excitation energies. Their analytic forms may not be available for arbitrary Δ_s and Δ_p , and therefore will be evaluated numerically in the rest of this paper.

Using the anti-commutation relationship between fermion operator, $\hat{\gamma}_{j,\mathbf{k}}$, and $\langle \hat{\gamma}_{j,\mathbf{k}}^\dagger \hat{\gamma}_{j,\mathbf{k}} \rangle = 0$ for the ground state expectation value, we could easily derive the mean-field ground state energy to be (combined with the constant term, E_c in Eq. (3))

$$E_G = E_C + \frac{1}{2} \sum_{j,\mathbf{k}} E_{j,\mathbf{k}} = \frac{1}{\Omega} \sum_{\mathbf{k},\mathbf{k}'} V_{\mathbf{k},\mathbf{k}'}^\perp \langle \hat{c}_{\mathbf{k}',\uparrow}^\dagger \hat{c}_{-\mathbf{k}',\downarrow}^\dagger \rangle \langle \hat{c}_{-\mathbf{k},\downarrow} \hat{c}_{\mathbf{k},\uparrow} \rangle + \frac{1}{\Omega} \sum_{\mathbf{k},\mathbf{k}'} V_{\mathbf{k},\mathbf{k}'}^\parallel \langle \hat{c}_{\mathbf{k}',\uparrow}^\dagger \hat{c}_{-\mathbf{k}',\uparrow}^\dagger \rangle \langle \hat{c}_{-\mathbf{k}\uparrow} \hat{c}_{\mathbf{k},\uparrow} \rangle + \frac{1}{\Omega} \sum_{\mathbf{k},\mathbf{k}'} V_{\mathbf{k},\mathbf{k}'}^\parallel \langle \hat{c}_{\mathbf{k}',\downarrow}^\dagger \hat{c}_{-\mathbf{k}',\downarrow}^\dagger \rangle \langle \hat{c}_{-\mathbf{k},\downarrow} \hat{c}_{\mathbf{k},\downarrow} \rangle + 2 \sum_{\mathbf{k}} \varepsilon_{\mathbf{k}} + \frac{1}{2} \sum_{j,\mathbf{k}} E_{j,\mathbf{k}} \quad (7)$$

From the expression above, one could see that the ground state energy depends on the ground state expectation value of the pairing operators, $\langle \hat{c}_{-\mathbf{k},\sigma} \hat{c}_{\mathbf{k},\sigma'} \rangle$, which also appears in the definition of the order parameter, $\Delta_s(\mathbf{k})$ and $\Delta_{p,\sigma}(\mathbf{k})$, see Eqs. (4) and (5). In this paper, we will use variational method to calculate the ground state energy by parametrizing these order parameters according to the lattice symmetry. More precisely, we could expand the intra- and inter-layer interaction as following:

$$V_{\mathbf{k},\mathbf{k}'}^{\parallel,\perp} = \sum_{mn \in Z} V_{mn}^{\parallel,\perp} \cos [m(k_x - k'_x)a + n(k_y - k'_y)a] \quad (8)$$

$$\Delta_s(\mathbf{k}) = \sum_{m,n \in Z} \Delta_{mn}^s [\cos(mk_x a + nk_y a) + \cos(nk_x a - mk_y a)] \quad (9)$$

$$\Delta_{p,\sigma}(\mathbf{k}) = \sum_{m,n \in Z} \Delta_{mn}^{p,\sigma} [\sin(mk_x a + nk_y a) - i \sin(nk_x a - mk_y a)] \quad (10)$$

$$\langle \hat{c}_{-\mathbf{k},\uparrow} \hat{c}_{\mathbf{k},\downarrow} \rangle = \sum_{m,n \in Z} c_{mn}^s [\cos(mk_x a + nk_y a) + \cos(nk_x a - mk_y a)] \quad (11)$$

$$\langle \hat{c}_{-\mathbf{k},\sigma} \hat{c}_{\mathbf{k},\sigma} \rangle = \sum_{m,n \in Z} c_{mn}^{p,\sigma} [\sin(mk_x a + nk_y a) - i \sin(nk_x a - mk_y a)] \quad (12)$$

Here Δ_{mn}^s , $\Delta_{mn}^{p,\sigma}$, c_{mn}^s and $c_{mn}^{p,\sigma}$ are all complex numbers, which could be determined later through a variational approach. m and n are integers for the index used in the reciprocal lattice. In the literature before, it is usually assumed that the pairing order parameters are proportional to the in-

teraction strengths for simplicity, but this assumption cannot be justified when considering the competition between order parameters. In order to consider these order parameters correctly, we note that Δ_{mn}^s and $\Delta_{mn}^{p,\sigma}$ could be calculated from c_{mn}^s and $c_{mn}^{p,\sigma}$ through the definition of gap function in Eqs.

(4) and (5). We will express their relationship in more details below for variational methods.

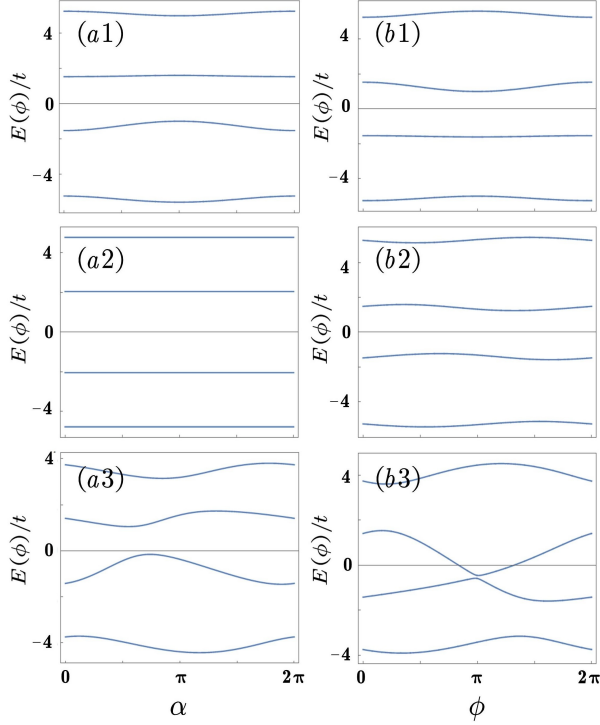


FIG. 2: (a1)-(a3) are eigenstate energies E_j of the BCS Hamiltonian in Eq. (6) as a function of the pairing phase, $\alpha = \alpha_\uparrow - \alpha_\downarrow$. (b1)-(b3) show the same results as a function of another pairing phase, $\phi = \phi_\uparrow - \phi_\downarrow$. Here $(k_x, k_y) = (0, \pi/2), (\pi/2, 0)$, and $(\pi/2, \pi/2)$ for the upper, middle and lower panels respectively. Other parameters are $\Delta_0^s/t = \Delta_1^p/t = 1$, $t_z/t = 2$, and $\mu/t = 1$.

B. Variational Approach and Pairing Phase Dependence of the Ground State Energy

Although the expression of order parameters above could be applied to a general finite ranged interaction, it is still much more intuitive and transparent to start with a finite range interaction range, i.e. $R_c \sim a, d$, with a and d being the intra-layer and inter-layer lattice spacing respectively. For such a finite ranged attractive interaction, it is reasonable for us to first consider the nearest neighboring terms of pairing only, i.e. $|m|, |n|, |m \pm n| \leq 1$, and neglect the longer-ranged pairing. Since our work is to emphasize the effects of these

pairing phases on the ground state properties, it is much more instructive to concentrate on the coupling between the nearest neighboring intra-layer and inter-layer pairing only. Including longer-ranged pairing requires much more pairing phases to be calculated self-consistently, and makes it difficult to interpret the mechanism. We will investigate the pairing phase dependence for this long-ranged interaction in the future. As a result, we could simplify the general expression of the gap functions in the last section and obtain,

$$\Delta_s(\mathbf{k}) = \Delta_0^s + \Delta_1^s [\cos(k_x a) + \cos(k_y a)] \quad (13)$$

$$\Delta_{p,\sigma}(\mathbf{k}) = 2ie^{i\phi_\sigma} \Delta_1^p [\sin(k_x a) + ie^{i\alpha_\sigma} \sin(k_y a)] \quad (14)$$

$$\langle \hat{c}_{-\mathbf{k},\uparrow} \hat{c}_{\mathbf{k},\downarrow} \rangle = c_0^s + c_1^s [\cos(k_x a) + \cos(k_y a)] \quad (15)$$

$$\langle \hat{c}_{-\mathbf{k},\sigma} \hat{c}_{\mathbf{k},\sigma} \rangle = 2ic_1^p [\sin(k_x a) + i \sin(k_y a)]. \quad (16)$$

Here we have set the pairing phase of the s -wave pairing order parameter to be zero, and separate the phases of these p -wave order parameters, so that $\Delta_{0,1}^s$, Δ_1^p , $c_{0,1}^s$ and c_1^p are all defined to be positive. α_σ and ϕ_σ are the four relative phases for the pairing order parameters as indicated above. Extension to a longer interaction range is straightforward but will not be considered in this paper.

Using the expression above, it is easy to directly connect the relationship between $\Delta_{0,1}^{s,p}$ and $c_{0,1}^{s,p}$ through the definition of order parameters in Eqs. (4) and (5). We have

$$\Delta_0^s = V_0^\perp c_0^s \quad (17)$$

$$\Delta_1^s = \frac{1}{2} V_1^\perp c_1^s \quad (18)$$

$$\Delta_1^p = \frac{1}{2} V_1^\parallel c_1^p \quad (19)$$

and therefore the mean-field ground state energy in Eq. (7) can be calculated directly to be

$$E_G = \sum_{\mathbf{k}} (2\zeta_{\mathbf{k}} - \frac{1}{2} \sum_j E_{j,\mathbf{k}}) + \frac{|\Delta_0^s|^2}{V_0^\perp} + \frac{2|\Delta_1^s|^2}{V_1^\perp} + \frac{2|\Delta_1^p|^2}{V_1^\parallel}$$

Here the three order parameters, $\Delta_{0,1}^s$ and Δ_1^p are then treated as independent variational parameters.

However, besides the magnitude of order parameters, the ground state energy also depends on the relative values between these pairing phases, $(\alpha_\uparrow, \alpha_\downarrow, \phi_\uparrow, \phi_\downarrow)$. They are embedded inside the expression of the Bogoliubov eigenstate energy, $E_{j,\mathbf{k}}$. We have examined all the possible combinations of these pairing phases, but present results only using their relative values, $\alpha \equiv \alpha_\uparrow - \alpha_\downarrow$ and $\phi \equiv \phi_\uparrow - \phi_\downarrow$ by setting $\alpha_\downarrow = \phi_\downarrow = 0$ in the rest of this paper. It is because this could give the most representative results without missing other information. As an example, we could analytically calculate the eigenvalues of Bogoliubov excitations for $(\alpha, \phi) = (0, 0)$ to be

$$E_{j,\mathbf{k}} = \pm \left[\varepsilon_{\mathbf{k}}^2 + t_z^2 + 4|\Delta_1^p|^2 (\sin^2(k_x a) + \sin^2(k_y a)) + |\Delta_0^s|^2 \pm 2\sqrt{\varepsilon_{\mathbf{k}}^2 t_z^2 + t_z^2 |\Delta_0^s|^2 + 4|\Delta_1^p|^2 |\Delta_0^s|^2 \sin^2(k_x a)} \right]^{1/2} \quad (20)$$

For $(\alpha, \phi) = (\pi, \pi)$, we have

$$E_{j,\mathbf{k}} = \pm \left[\varepsilon_{\mathbf{k}}^2 + t_z^2 + 4|\Delta_1^p|^2 (\sin^2(k_x a) + \sin^2(k_y a)) + |\Delta_0^s|^2 \pm 2|t_z| \sqrt{\varepsilon_{\mathbf{k}}^2 + |\Delta_0^s|^2 + 4|\Delta_1^p|^2 \sin^2(k_x a)} \right]^{1/2} \quad (21)$$

Analytical forms of these eigenstate energies could be also obtained in other specific values of (α, ϕ) . However, for a general value of (α, ϕ) , we will evaluate it numerically for the variational calculation below. In Fig. 2(a1)-(a3) and (b1)-(b3), we show how the numerically calculated eigenenergies changes as a function of these pairing phases.

C. The system symmetry

From the Anderson pseudo-spin point of view [37], the $SU(2)$ and Z_2 symmetries are broken explicitly in the BCS mean-field Hamiltonian (see Eq. (2)). Nevertheless, we find that, by selecting appropriate parameters, say $t_z = 0$, $\phi_{\uparrow} = -\phi_{\downarrow}$, and $\alpha_{\uparrow} = \pi + \alpha_{\downarrow}$, the bilayer system we study here becomes time-reversal symmetric. More precisely speaking, the chiral directions of the two superfluids in the upper and lower layers are opposite, making the time-reversal symmetry restored if reversing the parity in the z -axis. However, if the inter-layer tunneling is finite, such time-reversal symmetry disappears as expected, both in the original Hamiltonian and the mean-field one. In terms of the mean-field Hamiltonian, the pairing term in low energy limit can be expressed as $\Delta(k) = i\sigma_2(\Delta_s\sigma_0 + \Delta_p(k_x\sigma_1 + ie^{i\alpha}k_y\sigma_2))$. The value of α determines the time-reversal symmetry of the system. We find that in the self-consistent mean-field treatment, α can be π . The time-reversal operation $T := i\sigma_2 K$ maps $\Delta(k)$ to $\Delta(-k)$ indicates the preserving of the time-reversal symmetry. In our self-consistent mean-field treatment, we do not add other constraints besides the breaking of $U(1)$ symmetry. However, since the relative values of these phases may be pinned by the interaction effects, some symmetry (say the C_4 rotational symmetry of original Hamiltonian in the $x - y$ plane) may be also broken in the exotic phases we discussed in the context of Fig.5.

IV. QUANTUM PHASE DIAGRAM

A. Competition and Co-existence of s - and p -wave Order Parameters

In Fig. 3(a), we show the calculated quantum phase diagram in terms of the two pairing phases, α and ϕ . The result is obtained by a given set of system parameters, $V_0^{\perp}/t = 11$, $V_1^{\perp}/t = 5.8$, $V_1^{\parallel}/t = 6.2$, $t_z/t = 0.8$, and $\mu = 0.2$. The ground state is obtained by minimizing the ground state energy in the parameter space, $(\Delta_0^s, \Delta_1^s, \Delta_1^p)$. One can see that when the relative pairing phase between the two layers (i.e. α) is small, the ground state is mainly s -wave for $\phi \sim \pi/2$ and

becomes p -wave otherwise. The phase boundary between these two phases depend on α weakly. The transition between these two phases are found to be first order, as shown in Fig. 3(b). Such a result is reasonable because, when only the onsite inter-layer s -wave pairing is present (i.e. $\Delta_0^s \neq 0$, $\Delta_1^s = \Delta_1^p = 0$), all the pairing phase dependence of the ground state energy disappears. On the other hand, when the p -wave order parameters dominant, their relative phase respect to the s -wave also becomes unimportant, while the ground state energy strongly depends on the relative phase, ϕ , between the upper and lower layers. The lowest energy for small α regime stays at $\phi = 0, \pi$ as expected.

Note that, from energetic point of view, one could easily expect that the s -wave pairing will dominate as the two layers are very close (i.e. $d \ll a$), while the p -wave become dominant as the two layers are far away from each other (i.e. $d \gg a$). The phase diagram here is obtained by changing the pairing phases for a fixed value of d/a (here given by $t_z/t = 0.8$). Such pairing phase dependence in ground state energy could lead to a certain spontaneous phase transition, since these pairing phases are automatically determined by the interaction effects.

Besides the two traditional pairing mechanism shown above, we find that a hybrid ground state, where both Δ_0^s and Δ_1^p are finite (but within the parameter regime, $\Delta_1^s = 0$). It appears in a regime near $(\alpha, \phi) = (\pi, \pi)$, which was not investigated before. From the self-consistent mean-field calculation demonstrated here, the phase transition between this sp -coexisting ground state appears through a second order phase transition with a lower energy than either s -wave or p -wave states alone. The presence of such a sp -coexisting state is from the fact that near $(\alpha, \phi) = (\pi, \pi)$, Δ_0^s and Δ_1^p are coupled in a higher order terms in Landau's free energy expression through the complicated Bogoliubov excitation spectrum.

B. Quantum Phase Diagram in terms of the System Parameters

In order to investigate the phase diagram in terms of the realistic system parameters, we further express the quantum phase diagram in terms of interaction strengths, V_0^{\perp} and V_1^{\parallel} . The ground states are then determined by minimizing the full variational energy (E_G) in terms of three variational order parameter, $(\Delta_0^s, \Delta_1^s, \Delta_1^p)$, and two pairing phases, (α, ϕ) . Note that, both V_0^{\perp} and V_1^{\parallel} can be directly calculated from the full effective Rydberg-dressed interaction between dressed states. More generally, we analytically express their values in terms of a general inter-layer and intra-layer interaction, i.e. $V_0^{\perp} = V_{0,0}^{\perp}$, $V_1^{\perp} = V_{\pm 1,0}^{\perp} = V_{0,\pm 1}^{\perp}$, and $V_1^{\parallel} = V_{\pm 1,0}^{\parallel} = V_{0,\pm 1}^{\parallel}$,

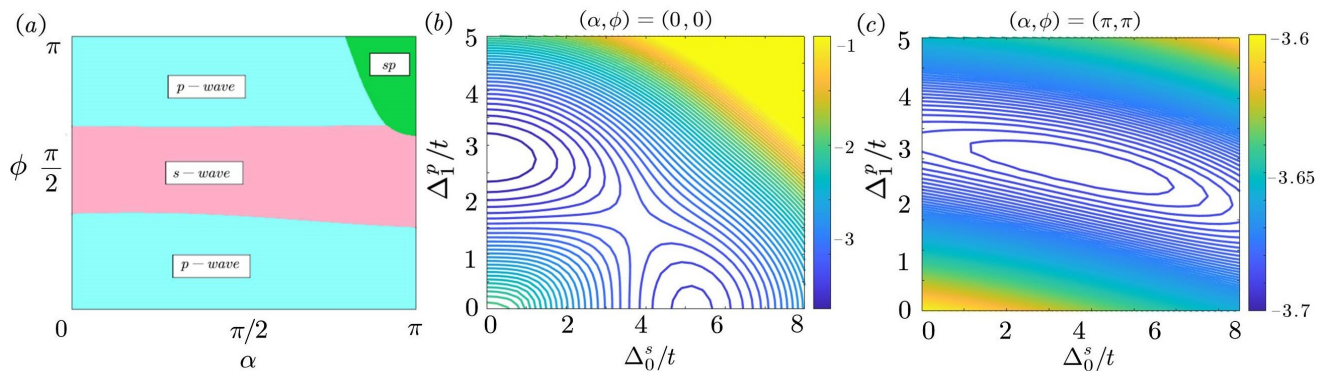


FIG. 3: (a) Diagrams of dominant pairing symmetry in terms of the pairing phase, (α, ϕ) , for $V_0^\perp/t = 11$, $V_1^\parallel/t = 6.2$ and $t_z/t = 0.8$, obtained by the self-consistent variational method.

The pink/blue area are for the s -wave/ p -wave pairing states, and the associated phase transitions between them are first order. The green area is the state with the coexistence of s - and p -waves at the same time, and its phase transition boundary with the other two phases are second order. (b) Variational energy contours for the pairing phase, $(\alpha, \phi) = (0, 0)$, as a function of Δ_0^s/t and Δ_1^p/t ($\Delta_1^s = 0$ for these cases). It shows two local minimum in the variational energy for the s -wave and p -wave states respectively. Their relative value determines the true ground state and hence provides a first order phase transition. (c) Same as (b) for $(\alpha, \phi) = (\pi, \pi)$. One could see that the energy minimum occurs at a point of finite values in Δ_0^s and Δ_1^p . It indicates the higher order coupling between the s -wave and p -wave order parameters.

where

$$V_{m,n}^\perp \equiv \frac{U_0}{[d^2 + (na)^2 + (ma)^2]^3 + R_c^6} \quad (22)$$

$$V_{m,n}^\parallel \equiv \frac{U_0}{[(na)^2 + (ma)^2]^3 + R_c^6} \quad (23)$$

with $n, m \in Z$ being the lattice site index. As a result, both V_1^\parallel and V_0^\perp can be tuned independently by changing U_0 and d , keeping the lattice constant a and the interaction range R_c the same. The value of inter-layer and inter-site interaction, V_1^\perp is then changed accordingly.

In Fig. 4, we show the calculated quantum phase diagram in terms of V_1^\parallel and V_0^\perp for $t_z/t = 0.8$ and $\mu/t = 0.2$. Several interesting and important properties could be observed: First, in the limit of zero interaction strength (white regime), there is no superfluid order parameter, because the finite inter-layer tunneling plays as a magnetic field to open a gap between different pseudo-spin components, suppressing the formation of Cooper pairs. In principle, the ground state could be a FFLO state due to the Fermi wavevector mis-matching, while we did not include this order parameters in our mean-field approach to simplify the calculation. This simplification is justified here because the critical temperature of the FFLO state is known much lower than regular superfluids due to its non-zero condensate momentum. (For example, the estimated T_c of such a FFLO state of $Na - Li$ polar molecules in a bilayer system is just about $10nK$ [36], well below the temperature current experiments.) Therefore, we believe our calculated quantum phase diagram should not be affected much even considering the FFLO state at a finite temperature.

Secondly, in the inter-mediate and stronger interaction regime, we observe the s - (p -wave) superfluid in the regime when V_0^\perp (V_1^\parallel) becomes dominant in the blue (pink) regime. This reflects the fact that this bilayer system has a great

flexibility to investigate the quantum phase transition between these two different superfluids via changing Rydberg-coupling strength or the inter-layer distance directly. As described above, the phase boundary between these two phases are first order without inter-mediate phase if the interaction is not strong.

However, in a stronger interaction regime, we do find the possibility to have a co-existing s -wave and p -wave superfluid, where the pairing phase becomes $(\alpha, \phi) = (\pi, \pi)$, as shown in the upper right corner of Fig. 3(a). We have to emphasize that, if one fixes the relative phases between s - and p -wave order parameters to be zero ($\alpha = \phi = 0$) as one usually did in the literature, we will not be able to find such a co-existing multi-order superfluidity from the variational approach. Although the regime of such an sp -coexisting phase seems not very large, it still provides an important route to investigate a new topological superfluidity, i.e. the traditional chiral p -wave superfluids could be coupled and paired together, making a possible new topological superfluid, which we will study in more details later.

V. GAPLESS TOPOLOGICAL SUPERFLUID

A. Band Structure and Edge States

Since we are more interested in the phase with the coexistence of both s - and p -wave superfluids, it will be more instructive to investigate its band structure and edge state properties first. In Fig. 5(a) we show the calculated band structure for $L_x = L_y = 100$ with a periodic boundary condition in both x and y directions. We have set $(\alpha, \phi) = (\pi, \pi)$ and find several gapless points in the band structure. Note that such gapless structure does not exist if the relative phases between these order parameters are the same (i.e. $\alpha = \phi =$

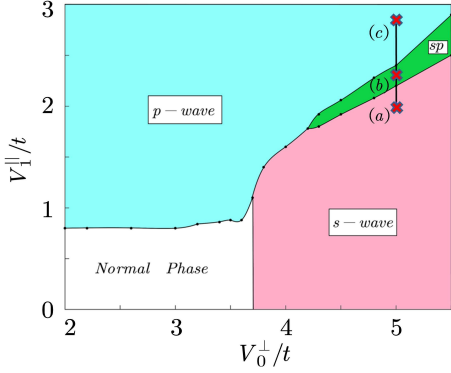


FIG. 4: Quantum phase diagram as a function of inter-layer and intra-layer interaction strengths, V_0^\perp/t and V_1^\parallel/t . The pink and blue area are ground states of s -wave and p -wave pairing order parameters only. The green area stands for the ground state with the co-existence of these two order parameters at the same time (with $(\alpha, \phi) = (\pi, \pi)$). In the white region, the ground state is a normal state without order parameters within our variational method. This is due to the presence of a finite interlayer tunneling and the competition between the s - and p -wave pairing state. Here we use $t_z = 0.8$. The vertical line and three cross points (labeled by (a), (b) and (c)) in the upper right corner are the points for the three finite temperature phase diagrams in Fig. 6.

0). In other words, the pairing phase modulation makes two gapped superfluids (s - and p -waves) co-exist and close their gaps, leading to interesting topological superfluid similar to nodal superconductors [38–42] as shown below.

To investigate if there could be any edge states due to the topological properties in the bulk, in Figs. 5(b) and (c), we show the calculated band structures with an open boundary condition in the y and x directions (i.e., k_x and k_y are good quantum numbers respectively). We could find that their band structures are very different due to the phase locking between the inter-layer pairing and the intra-layer pairing order parameters. More importantly, we could clearly find the localized state band energy in both sides. This reflects the bulk-edge corresponding principle of the topological matter. When the boundary is open in the y direction, the localized edge mode has a flat band, connecting different gapless points projected on the edge Brillouin zone, as shown in Fig. 5(b). As we will show below, this indicates the quantized topological charge for these gapless points.

B. Topological Charge of Gapless Points

In order to investigate the topological properties of this new phase in more details, here we calculate the possible topological charge of these gapless points, whose positions, (k_x^0, k_y^0) , could be calculated easily from the eigenmode spectrum, see Eq. (21). The gap is closed at $k_y^0 = 0, \pi$, and $\sqrt{\varepsilon_{\mathbf{k}^0}^2 + |\Delta_0^s|^2 + 4|\Delta_1^p|^2 \sin^2(k_x^0 a)} \pm t_z = 0$, leading to four

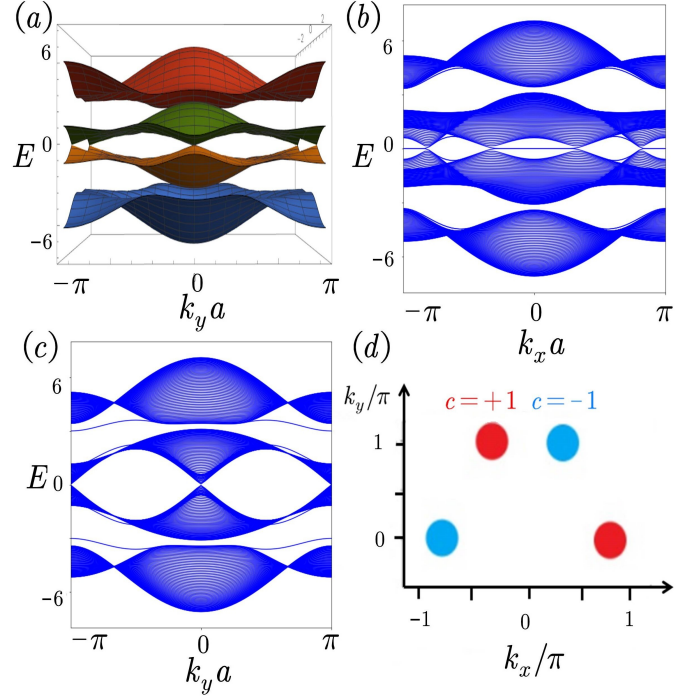


FIG. 5: (a) Band Structure of the the gapless topological superfluid calculated in a periodic boundary condition for $L_x = L_y = 100$. Here we use $\Delta_0^s/t = \Delta_1^p/t = 1$, $t_z/t = 2$, and $\mu/t = 1$. (b) Same as (a) but along the k_x direction with an open boundary condition in the y axis. (c) Same as (a) but along the k_y direction with an open boundary condition in the x axis. (d) shows the position of gapless points for the gapless topological superfluid. The gap-closing points with red/blue color indicate positive/negative charges for $W = +1/-1$.

solutions distributed in the momentum space as shown in Fig. 5(d). The red/blue colors indicate positive/negative topological charges as we will show below.

It is well-known [43–45] that in three dimensions, the topological charge is defined to be the surface integral of Berry curvature around a topological monopole, i.e. the Chern number. In two dimensionals, a loop that encircles the gapless point defines the topological charge, which is then equivalent to the winding number. There are several methods to calculate the topological charges around the gapless points. Here we note that the band disperses linearly in the momentum space through the gapless point, so that we could obtain the effective Hamiltonian around (k_x^0, k_y^0) up to the linear terms, i.e. $\mathbf{k} = \mathbf{k}^0 + \mathbf{q} + \mathcal{O}(q^2)$, and hence $\hat{H}(\mathbf{k}) = \hat{H}_0(\mathbf{k}^0) + \hat{H}_1(\mathbf{q}) + \mathcal{O}(q^2)$. Here zeroth order term of the Hamiltonian is

$$H_0(\mathbf{k}^0) = \varepsilon_{\mathbf{k}} (\sigma_3 \otimes \sigma_0) - \Delta_s (\sigma_2 \otimes \sigma_2) - t_z (\sigma_3 \otimes \sigma_1) - 2\Delta_p [\sin(k_x^0 a)] (\sigma_2 \otimes \sigma_0) - 2\Delta_p [\sin(k_y^0 a)] (\sigma_1 \otimes \sigma_3) \quad (24)$$

and the leading order Hamiltonian is

$$\begin{aligned} \hat{H}_1(\mathbf{q}) &= 2t[q_x \sin(k_x^0 a) + q_y \sin(k_y^0 a)] (\sigma_3 \otimes \sigma_0) \\ &\quad - 2\Delta_1^p q_x \cos(k_x^0 a) (\sigma_2 \otimes \sigma_0) \end{aligned} \quad (25)$$

Note that we use the direct product of two Pauli matrix for a general expression of the original 4×4 matrix.

In order to get the effective two-band Hamiltonian, we first numerically solve the 4×4 unperturbed Hamiltonian, $\hat{H}_0(\mathbf{k}^0)$, and express the leading order term, $\hat{H}_1(q)$, in this eigenstate basis. We then obtain the 2×2 effective Hamiltonian by projecting the original Hamiltonian to two bands near zero energy.

$$\begin{aligned} H_{eff}(\mathbf{q}) &= \begin{bmatrix} \langle v_1 | H_1(\mathbf{q}) | v_1 \rangle & \langle v_1 | H_1(\mathbf{q}) | v_2 \rangle \\ \langle v_2 | H_1(\mathbf{q}) | v_1 \rangle & \langle v_2 | H_1(\mathbf{q}) | v_2 \rangle \end{bmatrix} \\ &= v_x(\mathbf{k}^0) q_x \sigma'_x + v_y(\mathbf{k}^0) q_y \sigma'_y. \end{aligned} \quad (26)$$

In the last line, we have transformed the 2×2 matrix into a new basis, expressed by $\{\sigma'_x$ and $\sigma'_y\}$ in order to match the general form of gapless points with coefficients $v_x(\mathbf{k}^0)$ and $v_y(\mathbf{k}^0)$ respectively. In order to calculate the winding number around these gapless points more conveniently, we express the final effective Hamiltonian in polar coordinates by $v_x(\mathbf{k}^0) q_x = R(\mathbf{q}) \sin \theta_{\mathbf{q}} \cos \phi_{\mathbf{q}}$, $v_y(\mathbf{k}^0) q_y = R(\mathbf{q}) \sin \theta_{\mathbf{q}} \sin \phi_{\mathbf{q}}$, so that

$$H_{eff}(\mathbf{q}) = R(\mathbf{q}) \begin{pmatrix} 0 & e^{i\theta_{\mathbf{q}}} \\ e^{-i\theta_{\mathbf{q}}} & 0 \end{pmatrix} \quad (27)$$

with $R(\mathbf{q}) \equiv \sqrt{v_x(\mathbf{k}^0)^2 q_x^2 + v_y(\mathbf{k}^0)^2 q_y^2}$ and $\theta_{\mathbf{q}} \equiv \tan^{-1} \left[\frac{v_y(\mathbf{k}^0) q_y}{v_x(\mathbf{k}^0) q_x} \right]$. The corresponding winding number is then given by

$$W(\mathbf{k}^0) = \frac{1}{2\pi i} \oint d\theta_{\mathbf{q}} \partial_{\theta_{\mathbf{q}}} e^{i\theta_{\mathbf{q}}} = \pm 1, \quad (28)$$

depending on the positions of Weyl points. Note that due to the fermion-doubling theorem [46–49], the sum of all topological charges needs to be zero since topological point nodes with positive and negative values come in pairs.

In Fig. 5(d), we show the calculated results of topological charges for each gapless point in the momentum space. The bulk energy spectrum is shown in Fig. 5(a). It is clear that the points of positive charge and negative charge appears alternatively in space, while the breakdown of rotational C_4 symmetry makes the projection of total charge to be zero on the k_y axis, but non-zero on the k_x axis [see Figs. 5(b)(c)]. It explains why a zero mode appears in the edge state when the boundary is open in the y direction (hence k_x is a conserved quantum number), as shown in Fig. 5(b).

VI. FINITE-TEMPERATURE EFFECTS

After studying the quantum phase diagram at zero temperature, we further investigate the finite temperature effects of such a gapless topological superfluid, which has co-existing

s - and p -wave order parameters. The phases at a finite temperature can be obtained by minimizing the total Helmholtz free energy, $F(T) = E(T) - TS(T)$, where within the mean-field approximation, the energy $E(T) = \langle \hat{H}_{BCS} \rangle + E_C$ and the entropy $S(T)$ has to be calculated by including the thermal distribution of the Bogoliubov quasi-particles at a temperature T . Here the thermal expectation value of the BCS effective Hamiltonian is given by (see Eq. (6))

$$\begin{aligned} \langle \hat{H}_{BCS} \rangle &= \frac{1}{2} \sum_{\mathbf{k}} \left[E_{1,\mathbf{k}} \langle \hat{\gamma}_{1,\mathbf{k}}^\dagger \hat{\gamma}_{1,\mathbf{k}} \rangle + E_{2,\mathbf{k}} \langle \hat{\gamma}_{2,\mathbf{k}}^\dagger \hat{\gamma}_{2,\mathbf{k}} \rangle \right. \\ &\quad \left. + E_{3,\mathbf{k}} \langle \hat{\gamma}_{3,-\mathbf{k}}^\dagger \hat{\gamma}_{3,-\mathbf{k}} \rangle + E_{4,\mathbf{k}} \langle \hat{\gamma}_{4,-\mathbf{k}}^\dagger \hat{\gamma}_{4,-\mathbf{k}} \rangle \right] \\ &= \frac{1}{2} \sum_{\mathbf{k}} [E_{1,\mathbf{k}} f_{1,\mathbf{k}} + E_{2,\mathbf{k}} f_{2,\mathbf{k}} \\ &\quad + E_{3,\mathbf{k}} (1 - f_{3,-\mathbf{k}}) + E_{4,\mathbf{k}} (1 - f_{4,-\mathbf{k}})], \end{aligned} \quad (29)$$

where $E_{j,\mathbf{k}} (j = 1, \dots, 4)$ are the four eigenvalues of the BCS Hamiltonian. The quasi-particle thermal expectation is given by $\langle \hat{\gamma}_{j,\mathbf{k}}^\dagger \hat{\gamma}_{j,\mathbf{k}} \rangle = f_{j,\mathbf{k}}$ at the finite temperature, where $f_{j,\mathbf{k}} = \frac{1}{e^{E_{j,\mathbf{k}}/T} + 1}$ is the Fermi-Dirac distribution. Similarly, the entropy could be also calculated easily from these elementary excitations:

$$S(T) = - \sum_{j,\mathbf{k}} [f_{j,\mathbf{k}} \ln f_{j,\mathbf{k}} + (1 - f_{j,\mathbf{k}}) \ln (1 - f_{j,\mathbf{k}})]. \quad (30)$$

As a result, the finite temperature order parameter (i.e. $\Delta_0^s(T)$, $\Delta_1^s(T)$, and $\Delta_1^p(T)$) are now treated as a temperature dependent variational parameters to minimize the total Helmholtz free energy, $F(T)$, where both the constant energy, E_C , and the elementary excitation energy, $E_{j,\mathbf{k}}$, have such order parameter dependence as shown in Eqs. (3) and (20) respectively.

In Fig. 6(a) and (c) we show the results of the order parameters, $\Delta_0^s(T)$ and $\Delta_1^p(T)$, as a function of temperature inside the gapped superfluid phase, where $\Delta_1^p(T) \rightarrow 0$ and $\Delta_1^s(T) \rightarrow 0$ in these two parameter regimes. They correspond to (a) and (c) points in Fig. 4, where the pairing phases have been selected to be $(\alpha, \phi) = (\pi, \pi)$. (Note that when only s - or p -wave phase exists, there will be no pairing phase dependence in the energy and hence no difference if using other (α, ϕ) .) However, in the intermediate parameter regime, as shown in Fig. 6(b), these two order parameters could co-exist and changes in different way as a function of temperature. One could see that both s - and p -wave order parameters change non-monotonously as the temperature increases, and then decreases to zero at different critical temperature by thermal fluctuations, quite different from traditional superfluids with single order parameter only. The presence of two critical temperatures, $T_c^{s,p}$, also imply that there should be a *finite temperature* topological phase transitions in the intermediate temperature regime. In other words, the finite temperature topological phase transition indicates from a non-vanishing p -wave order parameter to vanishing p -wave order parameter in the presence of the coexisted s -wave order parameter. Note that, T_c^s could be either larger or smaller than T_c^p ,

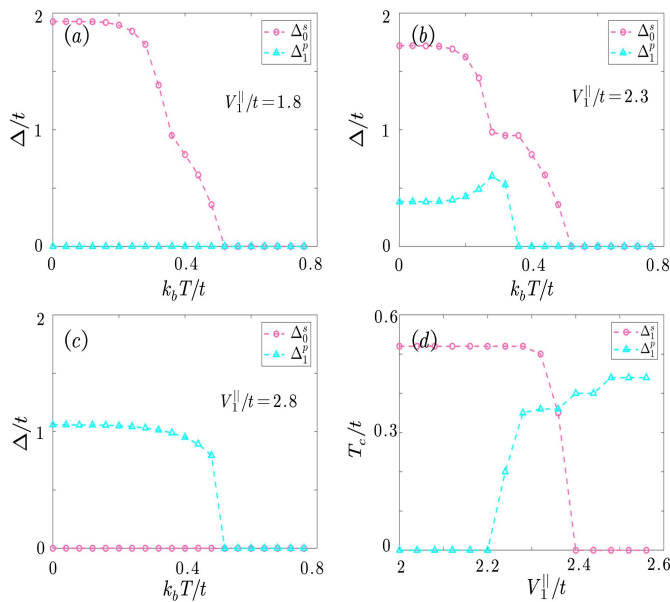


FIG. 6: (a) Temperature dependence of the s -wave pairing order parameter, $\Delta_0^s(T)$, and the p -wave pairing order parameter, $\Delta_1^p(T)$ in the parameter regime at the point (a) in Fig. 4. (b) and (c) are the same as (a), but with different interaction strength, see Fig. 4. (d) shows the critical temperature calculated as a function of V_1^{\parallel}/t for $V_0^{\perp}/t = 5$. There is a regime when both pairing exist with two critical temperatures.

depending on the parameters we consider within this gapless topological superfluid phase.

In Fig. 6(d), we show how the critical temperature of the two order parameters change as a function of intra-layer nearest neighboring interaction strength, V_1^{\parallel} , by keeping the interlayer on-site interaction, $V_0^{\perp}/t = 5$ along the vertical line in Fig. 4). One can see that the system is dominated by p -wave superfluid in one side and dominated by s -wave superfluid in the other side. In the intermediate regime, both of them exist and the associated phase is a gapless topological superfluid as we discussed above. We emphasize that such a result is obtained by a self-consistent mean-field approximation through the minimization of the total free energy for a given relative

pairing phase $(\alpha, \phi) = (\pi, \pi)$, and the co-existing result could not be obtained using other values of pairing phases, because the obtained free energy is higher than the present one. Therefore, by choosing proper pairing phases between these order parameters, the obtained gapless topological superfluid could exist not only at zero temperature but might also have highly non-trivial finite temperature effects.

VII. CONCLUSION

We systematically studied the ground state energy and quantum phase diagram of a 2D gapless topological superfluid. This topological system is constructed by a spin polarized fermionic atoms with a weakly coupling to Rydberg excited states in a bilayer optical lattice. Based on a self-consistent variational approximation, our numerical calculations show that the interlayer s -wave pairing and the intralayer p -wave pairing could co-exist in a parameter regime through a second order phase transition, if their relative pairing phases are modified spontaneously. We show that the obtained ground state is a gapless topological phases with a localized flat band in one of the edge. We further investigate the finite temperature phase diagram by minimizing the free energy. The competition between these two order parameters make a non-monotonic decrease of their order parameters, and the superfluid properties have two different critical temperatures. These interesting quantum and finite temperature many-body physics should be observable within the present experimental regimes.

VIII. ACKNOWLEDGEMENT

We thank Chung-Yu Mou, Chi-Ting Ho and Po-Hao Chou for insightful discussions. CYH is supported by the MOST of Taiwan under Grants No. 108-2112-M-029-006-MY3. PYC is supported by the MOST of Taiwan under Grants No. 111-2636-M-007-008. DWW is supported by the MOST of Taiwan under Grants No. 107-2112-M-007-019-MY3. This work is also supported by National Center for theoretical Sciences and by the Higher Education Sprout Project funded by the Ministry of Science and Technology and Ministry of Education in Taiwan.

[1] E. Majorana, Teoria simmetrica dell'elettrone e del positrone, Il Nuovo Cimento (1924-1942) **14**, 171 (2008).
 [2] A. Kitaev, Fault-tolerant quantum computation by anyons, Annals of Physics **303**, 2–30 (2003).
 [3] C. Nayak, S. H. Simon, A. Stern, M. Freedman, and S. Das Sarma, Non-abelian anyons and topological quantum computation, Reviews of Modern Physics **80**, 1083–1159 (2008).
 [4] S. D. Sarma, M. Freedman, and C. Nayak, Majorana zero modes and topological quantum computation, npj Quantum Information **1**, 1 (2015).

[5] X.-L. Qi and S.-C. Zhang, Topological insulators and superconductors, Reviews of Modern Physics **83**, 1057–1110 (2011).
 [6] A. Y. Kitaev, Unpaired majorana fermions in quantum wires, Physics-Uspekhi **44**, 131 (2001).
 [7] L. Fu and C. L. Kane, Superconducting proximity effect and majorana fermions at the surface of a topological insulator, Phys. Rev. Lett. **100**, 096407 (2008).
 [8] J. D. Sau, R. M. Lutchyn, S. Tewari, and S. Das Sarma, Generic new platform for topological quantum computation using semiconductor heterostructures, Phys. Rev. Lett. **104**, 040502 (2010).

- [9] E. Samuel Reich, A solid case for Majorana fermions, *Nature* **483**, 132 (2012).
- [10] J. Stajic, Looking for chiral majoranas, *Science* **367**, 36 (2020).
- [11] A. Banerjee, C. A. Bridges, J.-Q. Yan, A. A. Aczel, L. Li, M. B. Stone, G. E. Granroth, M. D. Lumsden, Y. Yiu, J. Knolle, S. Bhattacharjee, D. L. Kovrizhin, R. Moessner, D. A. Tennant, D. G. Mandrus, and S. E. Nagler, Proximate Kitaev quantum spin liquid behaviour in a honeycomb magnet, *Nature Materials* **15**, 733 (2016).
- [12] D. Wang, L. Kong, P. Fan, H. Chen, S. Zhu, W. Liu, L. Cao, Y. Sun, S. Du, J. Schneeloch, R. Zhong, G. Gu, L. Fu, H. Ding, and H.-J. Gao, Evidence for Majorana bound states in an iron-based superconductor, *Science* **362**, 333 (2018).
- [13] M. Kayyalha, D. Xiao, R. Zhang, J. Shin, J. Jiang, F. Wang, Y.-F. Zhao, R. Xiao, L. Zhang, K. M. Fijalkowski, P. Mandal, M. Winnerlein, C. Gould, Q. Li, L. W. Molenkamp, M. H. W. Chan, N. Samarth, and C.-Z. Chang, Absence of evidence for chiral Majorana modes in quantum anomalous Hall-superconductor devices, *Science* **367**, 64 (2020).
- [14] D. Castelvecchi, Evidence of elusive majorana particle dies - but computing hope lives on, *Nature* **591**, 354 (2021).
- [15] L. Jiang, T. Kitagawa, J. Alicea, A. R. Akhmerov, D. Pekker, G. Refael, J. I. Cirac, E. Demler, M. D. Lukin, and P. Zoller, Majorana fermions in equilibrium and in driven cold-atom quantum wires, *Physical Review Letters* **106**, 10.1103/physrevlett.106.220402 (2011).
- [16] S. Tewari, S. Das Sarma, C. Nayak, C. Zhang, and P. Zoller, Quantum computation using vortices and majorana zero modes of a $p_x + ip_y$ superfluid of fermionic cold atoms, *Phys. Rev. Lett.* **98**, 010506 (2007).
- [17] Z. Shermadini, A. Krzton-Maziopa, M. Bendele, R. Khasanov, H. Luetkens, K. Conder, E. Pomjakushina, S. Weyeneth, V. Pomjakushin, O. Bossen, and A. Amato, Coexistence of magnetism and superconductivity in the iron-based compound $\text{Cs}_{0.8}(\text{fese}_{0.98})_2$, *Phys. Rev. Lett.* **106**, 117602 (2011).
- [18] X.-J. Liu, K. T. Law, and T. K. Ng, Realization of 2d spin-orbit interaction and exotic topological orders in cold atoms, *Phys. Rev. Lett.* **112**, 086401 (2014).
- [19] M. Sato, Y. Takahashi, and S. Fujimoto, Non-abelian topological order in s -wave superfluids of ultracold fermionic atoms, *Phys. Rev. Lett.* **103**, 020401 (2009).
- [20] C.-Y. Huang, J. Zhuang, P.-Y. Chang, and D.-W. Wang, Two-dimensional paired topological superfluids of rydberg fermi gases (2021), arXiv:2112.14027 [cond-mat.supr-con].
- [21] A. Pikovski, M. Klawunn, G. V. Shlyapnikov, and L. Santos, Interlayer superfluidity in bilayer systems of fermionic polar molecules, *Physical Review Letters* **105**, 10.1103/physrevlett.105.215302 (2010).
- [22] N. T. Zinner, B. Wunsch, D. Pekker, and D.-W. Wang, BCS-BEC crossover in bilayers of cold fermionic polar molecules, *Physical Review A* **85**, 10.1103/physreva.85.013603 (2012).
- [23] M. Babadi and E. Demler, Collective phenomena in a quasi-two-dimensional system of fermionic polar molecules: Band renormalization and excitons, *Physical Review A* **84**, 10.1103/physreva.84.033636 (2011).
- [24] M. A. Baranov, A. Micheli, S. Ronen, and P. Zoller, Bilayer superfluidity of fermionic polar molecules: Many-body effects, *Physical Review A* **83**, 10.1103/physreva.83.043602 (2011).
- [25] F. Cinti, D.-W. Wang, and M. Boninsegni, Phases of dipolar bosons in a bilayer geometry, *Physical Review A* **95**, 10.1103/physreva.95.023622 (2017).
- [26] A. C. Potter, E. Berg, D.-W. Wang, B. I. Halperin, and E. Demler, Superfluidity and dimerization in a multilayered system of fermionic polar molecules, *Physical Review Letters* **105**, 10.1103/physrevlett.105.220406 (2010).
- [27] C.-Y. Huang, Y.-T. Lin, H. Lee, and D.-W. Wang, Quantum degenerate majorana surface zero modes in two-dimensional space, *Phys. Rev. A* **99**, 043624 (2019).
- [28] N. Henkel, R. Nath, and T. Pohl, Three-Dimensional Roton Excitations and Supersolid Formation in Rydberg-Excited Bose-Einstein Condensates, *Physical Review Letters* **104**, 195302 (2010).
- [29] J. Honer, H. Weimer, T. Pfau, and H. P. Büchler, Collective Many-Body Interaction in Rydberg Dressed Atoms, *Physical Review Letters* **105**, 160404 (2010).
- [30] W. Li, L. Hamadeh, and I. Lesanovsky, Probing the interaction between Rydberg-dressed atoms through interference, *Physical Review A* **85**, 053615 (2012).
- [31] M. Płodzień, G. Lochead, J. de Hond, N. J. van Druten, and S. Kokkelmans, Rydberg dressing of a one-dimensional Bose-Einstein condensate, *Physical Review A* **95**, 043606 (2017).
- [32] G. Pupillo, A. Micheli, M. Boninsegni, I. Lesanovsky, and P. Zoller, Strongly Correlated Gases of Rydberg-Dressed Atoms: Quantum and Classical Dynamics, *Physical Review Letters* **104**, 223002 (2010).
- [33] D. Tong, S. M. Farooqi, J. Stanojevic, S. Krishnan, Y. P. Zhang, R. Côté, E. E. Eyler, and P. L. Gould, Local Blockade of Rydberg Excitation in an Ultracold Gas, *Physical Review Letters* **93**, 063001 (2004).
- [34] M. Saffman, T. G. Walker, and K. Mølmer, Quantum information with Rydberg atoms, *Reviews of Modern Physics* **82**, 2313 (2010).
- [35] A. Browaeys, D. Barredo, and T. Lahaye, Experimental investigations of dipole-dipole interactions between a few Rydberg atoms, *Journal of Physics B: Atomic, Molecular and Optical Physics* **49**, 152001 (2016).
- [36] H. Lee, S. I. Matveenko, D.-W. Wang, and G. V. Shlyapnikov, Fulde-ferrell-larkin-ovchinnikov state in bilayer dipolar systems, *Phys. Rev. A* **96**, 061602 (2017).
- [37] P. W. Anderson, Random-phase approximation in the theory of superconductivity, *Phys. Rev.* **112**, 1900 (1958).
- [38] S. Matsuura, P.-Y. Chang, A. P. Schnyder, and S. Ryu, Protected boundary states in gapless topological phases, *New Journal of Physics* **15**, 065001 (2013).
- [39] M. Sato, Nodal structure of superconductors with time-reversal invariance and \mathbf{z}_2 topological number, *Phys. Rev. B* **73**, 214502 (2006).
- [40] M. Sato, Y. Tanaka, K. Yada, and T. Yokoyama, Topology of andreev bound states with flat dispersion, *Phys. Rev. B* **83**, 224511 (2011).
- [41] M. Sato and S. Fujimoto, Existence of majorana fermions and topological order in nodal superconductors with spin-orbit interactions in external magnetic fields, *Phys. Rev. Lett.* **105**, 217001 (2010).
- [42] Y. Tanaka, Y. Mizuno, T. Yokoyama, K. Yada, and M. Sato, Anomalous andreev bound state in noncentrosymmetric superconductors, *Phys. Rev. Lett.* **105**, 097002 (2010).
- [43] T. Morimoto and A. Furusaki, Weyl and dirac semimetals with \mathbf{Z}_2 topological charge, *Phys. Rev. B* **89**, 235127 (2014).
- [44] P.-Y. Chang and P. Coleman, Parity-violating hybridization in heavy weyl semimetals, *Phys. Rev. B* **97**, 155134 (2018).
- [45] X. Wan, A. M. Turner, A. Vishwanath, and S. Y. Savrasov, Topological semimetal and fermi-arc surface states in the electronic structure of pyrochlore iridates, *Phys. Rev. B* **83**, 205101 (2011).
- [46] H. Nielsen and M. Ninomiya, Absence of neutrinos on a lattice: (i). proof by homotopy theory, *Nuclear Physics B* **185**, 20 (1981).

- [47] N. P. Armitage, E. J. Mele, and A. Vishwanath, Weyl and dirac semimetals in three-dimensional solids, *Rev. Mod. Phys.* **90**, 015001 (2018).
- [48] B. Béri, Topologically stable gapless phases of time-reversal-invariant superconductors, *Phys. Rev. B* **81**, 134515 (2010).
- [49] C. Fang and L. Fu, New classes of topological crystalline insulators having surface rotation anomaly, *Science Advances* **5**, eaat2374 (2019).